Centro Euro-Mediterraneo sui Cambiamenti Climatici

Research Papers
Issue RP0280
December 2015

ODA - Ocean modeling and Data Assimilation Division

Diurnal internal Tides along the Italian Coast of the Southern Adriatic Sea

By **Dong Wang**
Fondazione CMCC – Centro Euro-Mediterraneo sui Cambiamenti Climatici

Nadia Pinardi
Department of Physics and Astronomy, Alma Mater Studiorum, University of Bologna

n.pinardi@sincem.unibo.it

SUMMARY The occurrence of internal tides along the Italian coastline of the Adriatic Sea during the stratification season is revealed by a high-resolution, state-of-the-art, three-dimensional primitive-equation baroclinic tidal ocean model of the Adriatic Sea. The important semi-diurnal and diurnal tidal components for the Adriatic Sea are simulated by imposing tidal elevations and velocities along the model domain's southern boundary. The co-tidal charts and harmonics of tidal sea levels and phases of semi-diurnal and diurnal tides are well reproduced by the model, suggesting that the hydrodynamics key to tidal processes in the Adriatic are correctly represented. Vertical oscillations of isotherms near diurnal frequencies are evident at sites along the Italian coastline during the stratification season. Such vigorous oscillations are absent when the tidal forcing is removed. The occurrence of internal tides is readily explained by the supercritical slope theory.

Keywords: Tidal motion, Adriatic Sea, internal tides

The research leading to these results has received funding from the Italian Ministry of Education, University and Research and the Italian Ministry of Environment, Land and Sea under the GEMINA project for the OOCC China-Italy collaboration.

1. INTRODUCTION

Internal tides, or internal waves near the tidal frequencies, are generated when stratified waters flow over sloping bathymetry due to tidal motions [Huthnance, 1989]. In the global ocean internal tides act as a means by which barotropic tidal energy is dissipated and supplied to mixing [Munk and Wunsch, 1998]. The Adriatic Sea, a semi-enclosed basin connected to the Mediterranean through the Otranto strait, was once believed not to have internal tides due to the small barotropic tidal signal in the basin. Existence of diurnal internal tides in the stratification season has been reported around an island (Lastovo) along the Croatian coast where large amplitude isotherm vertical oscillations have been measured by in situ observations [Mihanovic et al., 2006; 2009]. Occasionally, superimposed to the tidally-driven vertical oscillation of isotherms is the prominent effect of episodically strong sea breeze cycles [Orlic et al., 2011], complicating the internal tide characteristics.

Internal tides in the Adriatic Sea have not been as systematically studied as the barotropic tides [Cushman-Roisin et al., 2001]. Furthermore, observations are not sufficiently dense in space and time to detect internal tides in the overall Adriatic Sea. Baroclinic circulation processes associated with barotropic tidal processes were first studied in the Adriatic Sea by Guarnieri et al. [2013], but the model vertical resolution (31 sigma layers) was not adequate to resolve internal tides. In the present study, we use a state-of-the-art primitive-equation ocean model with very high vertical resolution in the surface layers to study internal tides in the Adriatic Sea. The numerical experiments not only reproduce the diurnal internal tides around Lastovo island near the Croatian coast as revealed by the in-situ observations, but also suggest the existence of internal tides at other sites near the Italian coastlines.

Details of the model experiments are given in section 2. In section 3, major components of the diurnal and semi-diurnal frequency tides, are first compared with tide gauge observations along the Italian coast and accredited barotropic or baroclinic

tidal models of the Adriatic Sea. The simulated characteristics of internal tides are then described and discussed in section 4.

2. METHODOLOGY

The model used in this study is the NEMO (Nucleus for European Modelling of the Ocean, http://www.nemo-ocean.eu) model, a state-of-the-art modeling framework for oceanographic research, operational oceanography, seasonal forecast and climate studies. The model domain covers the whole Adriatic Sea, and extends to its southern boundary at 39°N of the northern Ionian Sea (Fig. 1). The horizontal resolution is 1/48°, which is approximately 2 km at this latitude. The model uses partial-cell z-coordinate with 120 layers in the vertical, with very high (1 m) resolution in the upper 60 m to resolve the thermocline physics, and the bottom layer is no thicker than 70 m in the deepest basin of the northern Ionian Sea where the open boundary resides. Atmospheric forcing of the ECMWF ERA-interim [Dee et al., 2011] data is supplied to the model at time intervals of 6 hours. The model set-up is the same as in Gunduz et al. [2014], except that in the present study tides and atmospheric pressure have been added.

The tidal forcing, including both the tidal elevation and the tidal velocities, is implemented at the southern boundary of the NEMO model domain (the 39°N line in the northern Ionian Sea, see Fig. 1) in the way specified in Guarnieri et al. [2013]. The tidal elevation and velocities at the model boundary are obtained using a regional version of the OTPS tidal model (Oregon State University Tidal Prediction Software: http://volkov.oce.orst.edu/tides/otps.html, Egbert and Erofeeva [2002]), which was specially developed for the Mediterranean Sea at a resolution of 1/30°. The time-splitting method for the explicit free surface and the total velocity equations is used, with a baroclinic timestep of 240 s and barotropic timestep of 3 s.

3. RESULTS

3.1. SEA LEVEL TIDAL COMPONENTS

3.1.1 COMPARISON OF CO-TIDAL CHARTS WITH PREVIOUS STUDIES

The dynamics of the semi-diurnal tides in the Adriatic Sea was successfully interpreted nearly a century ago by Taylor [1922] as incident and reflected Kelvin waves superimposed by a set of Poincare waves. The dynamical essence of the diurnal tides, however, had not been revealed until the beginning of this century by Malacic et al. [2000], who interpreted the diurnal tides as topographic waves. The cotidal charts obtained from the simulated sea level for both the semi-diurnal and diurnal tides (Fig. 2) are quite similar to those obtained with accredited barotropic and baroclinic models in the literature [Cushman-Roisin and Naimie, 2002; Guarnieri et al., 2013], indicating that the hydrodynamic processes key to tidal processes are well reproduced. As the largest and an example of semi-diurnal tides, the cotidal chart for M2 constitutes spider-net-like patterns in the northern Adriatic, with co-range lines circling the amphidromic point (Fig. 2a). The amplitudes increase away from the amphidromic points to the coast as the Kelvin waves are trapped by the coast. The cotidal chart for K1, the largest diurnal tide, displays fishnet-like patterns (Fig. 2b), with co-range lines crossing the basin while the co-phase lines somewhat parallel to the major axis of the basin.

3.1.2 COMPARISON WITH TIDE GAUGE OBSERVATIONS

The difference of modeled amplitudes from observations for M2, the largest semi-diurnal tide, is on average 8% for the eight tide gauges (Table 1), whereas such difference is 4% for tidal phases. The modeled amplitude of M2 reaches 24.37 cm, being 7% smaller than the observed, at Trieste, where the largest tides are seen in the Adriatic. The barotropic model used by Cushman-Roisin and Naimie [2002]

underestimated the M2 amplitude by 8% for this tide gauge, while Guarnieri et al. [2013] underestimated by 1%, with tidal elevation amplified by 10% at the open boundary.

In terms of phase estimation for diurnal tides the model demonstrates very good skills, with modeled K1 phase being on average 3% different from observations at the tide gauges (Table 1). Thus, we conclude that the model in the present study possesses tidal simulation skills comparable to, if not better than, those of contemporary numerical models of various types.

3.2. INTERNAL TIDES

3.2.1 SIMULATED INTERNAL TIDES NEAR THE CROATIAN COAST

Clear presence of internal tides can be seen from the simulated temperature time series at the model grid point nearest to Cape Struga of Lastovo Island. Fig. 3a shows that stratification (in this case mainly due to differences in temperatures among the three depths) commenced in the beginning of April. Significant diurnal oscillation of temperatures started since late April. Stratification and the diurnal internal tide damped and ceased at the end of August. Although they are for different period, a comparison against in-situ observations between March 2001 and March 2002 reported by Mihanovic et al. [2006] and reproduced here in Fig. 3b shows that our model simulation captured, qualitatively at least, the essential features of the diurnal internal tide around the Lastovo Island in the summer season, despite the crude representation of the finer features of topography, and that the model grid point is at some distance away from the Cape Struga observation site (Fig 1).

3.2.2 SIMULATED INTERNAL TIDES NEAR THE ITALIAN COAST

In Fig. 3c the power spectral density of temperature variations is shown at 30 m depth. An interesting feature revealed by the model is that in the strip southeast of the Gargano Peninsula and around the southern tip of the Apulian Peninsula, a considerably large portion of the thermocline depth variations can be attributed to diurnal frequencies. Other sites in the two Croatian archipelagos (Fig. 1) are found to be characterized by high energy internal tides but the largest amplitudes are along the southern Italian coastlines.

Figs. 4a and 4d show the temporal evolution in July 2006 of the vertical thermal structure of the two model grid points at locations shown with green and magenta diamonds in Fig. 1, respectively. The daily vertical oscillations of isotherms suggest the existence of large amplitude diurnal internal tides in these regions. The importance of the tidal forcing on internal tide generation is illustrated in Figs. 4b and 4e, which show the temporal evolution of the vertical thermal structure of at the same locations in a model simulation without tidal forcing at the open boundary. The significantly damped diurnal vertical isotherms oscillation in Figs 4b and 4e suggests that mechanisms other than tidal forcing are in this case of minor importance in generating internal tides.

The occurrence of internal tides can be readily explained with the supercritical slope theory. This dynamics was first developed theroretically by Wunsch [1968] and later verified in laboratory studies by Cacchione and Wunsch [1974]. Although the theory was originally for the situation of constant Brunt-Vaisala frequency and linear bottom slope, the theory sheds some light on the underlying dynamics of internal tides at these sites. Effects of rotation can be added to the theory as discussed in Huthnance [1989]. The topographic slopes along the two sections are compared against the critical slopes, which are calculated as

$$s = \left|\frac{\sigma^2 - f^2}{N^2 - \sigma^2}\right|^{1/2} \qquad (1)$$

where σ is the tidal frequency, f the local inertial frequency, and N the Brunt-Vaisala frequency. Figs 4c and 4f show that the topographic slopes along the sections crossing the bathymetry contours and containing the model grid points indeed exceed the calculated critical slopes.

4. DISCUSSION AND CONCLUSIONS

In this paper we have demonstrated that a high-resolution baroclinic tidal model is capable of properly simulating barotropic tides in the Adriatic Sea revealing the features of internal tide energy distribution around the Adriatic Sea. High internal tide energy is found along the croatian coastlines, in particular the two Croatian archipelagos in the middle and northern Adriatic Sea. Given that the presence of internal tides near the Croatian coast have been successfully reproduced by our model with respect to in situ observations, we believe that the distribution of internal tide energy is likely to be realistic. The Gargano peninsula and the Apulia coastlines down to the Otranto Strait are shown for the first time to be the site of intense internal tidal motion. Recently internal tides were detected from mooring data also in the Strait of Otranto [Ursella et al., 2014], which is very close to Section 2 of this study. We hope our numerical findings will be able to provide hints for future field experiment design, and study the possible internal wave breaking on the shelf break and impact on the Adriatic Sea circulation.

ACKNOWLEDGEMENTS

The research leading to these results has received funding from the Italian Ministry of Education, University and Research and the Italian Ministry of Environment, Land and Sea under the GEMINA project for the OOCC China-Italy collaboration.

BIBLIOGRAPHY

Cacchione, D., and C. Wunsch (1974), Experimental study of internal waves over a slope, J. Fluid Mech., 66(02), 223, doi:10.1017/S0022112074000164.

Cushman-Roisin, B., and C. E. Naimie (2002), A 3D finite-element model of the Adriatic tides, J. Mar. Syst., 37(4), 279–297, doi:10.1016/S0924-7963(02)00204-X.

Cushman-Roisin, B., V. Malačič, and M. Gačić (2001), Tides, Seiches and Low-Frequency Oscillations, in Physical Oceanography of the Adriatic Sea SE - 7, edited by B. Cushman-Roisin, M. Gačić, P.-M. Poulain, and A. Artegiani, pp. 217–240, Springer Netherlands.

Dee, D. P. et al. (2011), The ERA-Interim reanalysis: configuration and performance of the data assimilation system, Q. J. R. Meteorol. Soc., 137(656), 553–597, doi:10.1002/qj.828.

Egbert, G. D., and S. Y. Erofeeva (2002), Efficient Inverse Modeling of Barotropic Ocean Tides, J. Atmos. Ocean. Technol., 19(2), 183–204, doi:10.1175/1520-0426(2002)019<0183:EIMOBO>2.0.CO;2.

Guarnieri, A., N. Pinardi, P. Oddo, G. Bortoluzzi, and M. Ravaioli (2013), Impact of tides in a baroclinic circulation model of the Adriatic Sea, J. Geophys. Res. Ocean., 118(1), 166–183, doi:10.1029/2012JC007921.

Gunduz, M., S. Dobricic, P. Oddo, N. Pinardi, and A. Guarnieri (2013), Impact of Levantine Intermediate Water on the Interannual Variability of the Adriatic Sea based on simulations with a Fine Resolution Ocean Model, Ocean Model., 72(October), 253–263, doi:10.1016/j.ocemod.2013.10.002.

Huthnance, J. M. (1989), Internal tides and waves near the continental shelf edge, Geophys. Astrophys. Fluid Dyn., 48(1-3), 81–106, doi:10.1080/03091928908219527.

Malačič, V., D. Viezzoli, and B. Cushman-Roisin (2000), Tidal dynamics in the northern Adriatic Sea, J. Geophys. Res., 105(C11), 26265, doi:10.1029/2000JC900123.

Mihanović, H., M. Orlić, and Z. Pasarić (2006), Diurnal internal tides detected in the Adriatic, Ann. Geophys., 24(11), 2773–2780, doi:10.5194/angeo-24-2773-2006.

Mihanović, H., M. Orlić, and Z. Pasarić (2009), Diurnal thermocline oscillations driven by tidal flow around an island in the Middle Adriatic, J. Mar. Syst., 78, S157–S168, doi:10.1016/j.jmarsys.2009.01.021.

Munk, W., and C. Wunsch (1998), Abyssal recipes II: energetics of tidal and wind mixing, Deep Sea Res. Part I Oceanogr. Res. Pap., 45(12), 1977–2010, doi:10.1016/S0967-0637(98)00070-3.

Orlić, M., G. Beg Paklar, V. Dadić, N. Leder, H. Mihanović, M. Pasarić, and Z. Pasarić (2011), Diurnal upwelling resonantly driven by sea breezes around an Adriatic island, J. Geophys. Res., 116(C9), C09025, doi:10.1029/2011JC006955.

Taylor, G. I. (1922), Tidal Oscillations in Gulfs and Rectangular Basins, Proc. London Math. Soc., s2-20(1), 148–181, doi:10.1112/plms/s2-20.1.148.

Ursella, L., V. Kovačević, and M. Gačić (2014), Tidal variability of the motion in the Strait of Otranto, Ocean Sci., 10(1), 49–67, doi:10.5194/os-10-49-2014.

Wunsch, C. (1968), On the propagation of internal waves up a slope, Deep Sea Res. Oceanogr. Abstr., 15(3), 251–258, doi:10.1016/0011-7471(68)90002-8.

Table

Table 1. Observed, model simulated, and their differences of major tidal harmonics for amplitudes and phases at tide gauges.

	M2						K1					
	Amplitudes (cm)			Phases (°)			Amplitudes (cm)			Phases (°)		
Station	obs	mod	%diff	obs	mod	%diff	obs	mod	%diff	obs	mod	%diff
Ancona	6.56	4.84	26	326.7	342.9	9	12.95	10.28	21	81.5	87.2	3
Bari	9.84	9.53	3	104.0	109.3	3	4.92	4.14	16	64.4	68.9	3
Ortona	6.77	7.03	4	90.0	101.1	6	8.83	7.20	18	79.0	84.5	3
Otranto	6.86	7.28	6	102.9	107.9	3	2.30	2.12	8	72.3	63.1	5
Ravenna	16.83	15.20	10	298.6	304.4	3	15.94	12.84	19	78.5	82.8	2
Trieste	26.29	24.37	7	277.8	280.9	2	17.78	14.39	19	67.3	72.6	3
Venezia	23.86	22.16	7	287.2	290.9	2	17.50	14.05	20	73.4	77.3	2
Vieste	9.49	9.37	1	99.9	106.1	3	5.23	4.20	20	83.4	92.0	5
Ave Diff (%)			8			4			18			3

Figure 1. The model domain (12-19°E, 39-46°N) with bathymetry contours (50, 100, 200, 500 and 1000 m). The open boundary at 39°N in the northern Ionian Sea is shown by a thick blue line. Positions of tide gauges are shown in red dots. Sections 1 and 2 are shown in thin blue lines, with the two model grid points on them shown in green and magenta diamonds, respectively. The inlet shows a zoomed view of the red box, in which the observation site of Mihanovic et al. [2006] is shown by a red dot, and the model grid point for comparison is shown by a blue diamond.

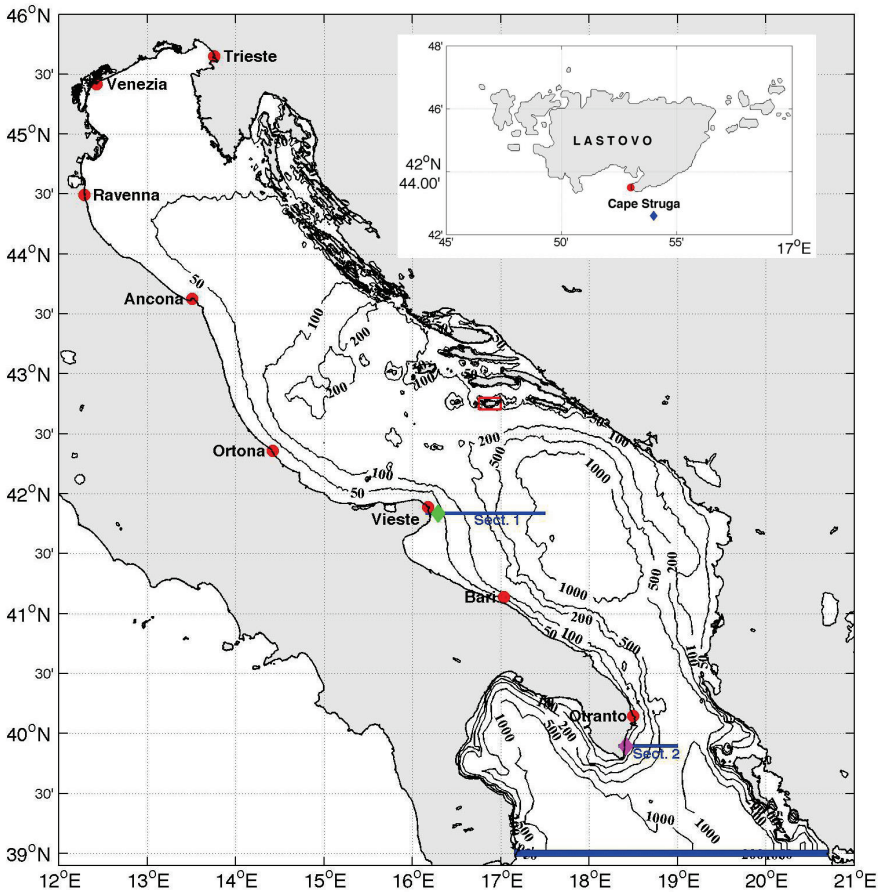

Figure 2. Cotidal charts for M2 (panel a) and K1 (panel b). Solid lines delineate co-range lines (of the same tidal amplitude), and long-dashed lines the co-phase lines (of the same tidal phase).

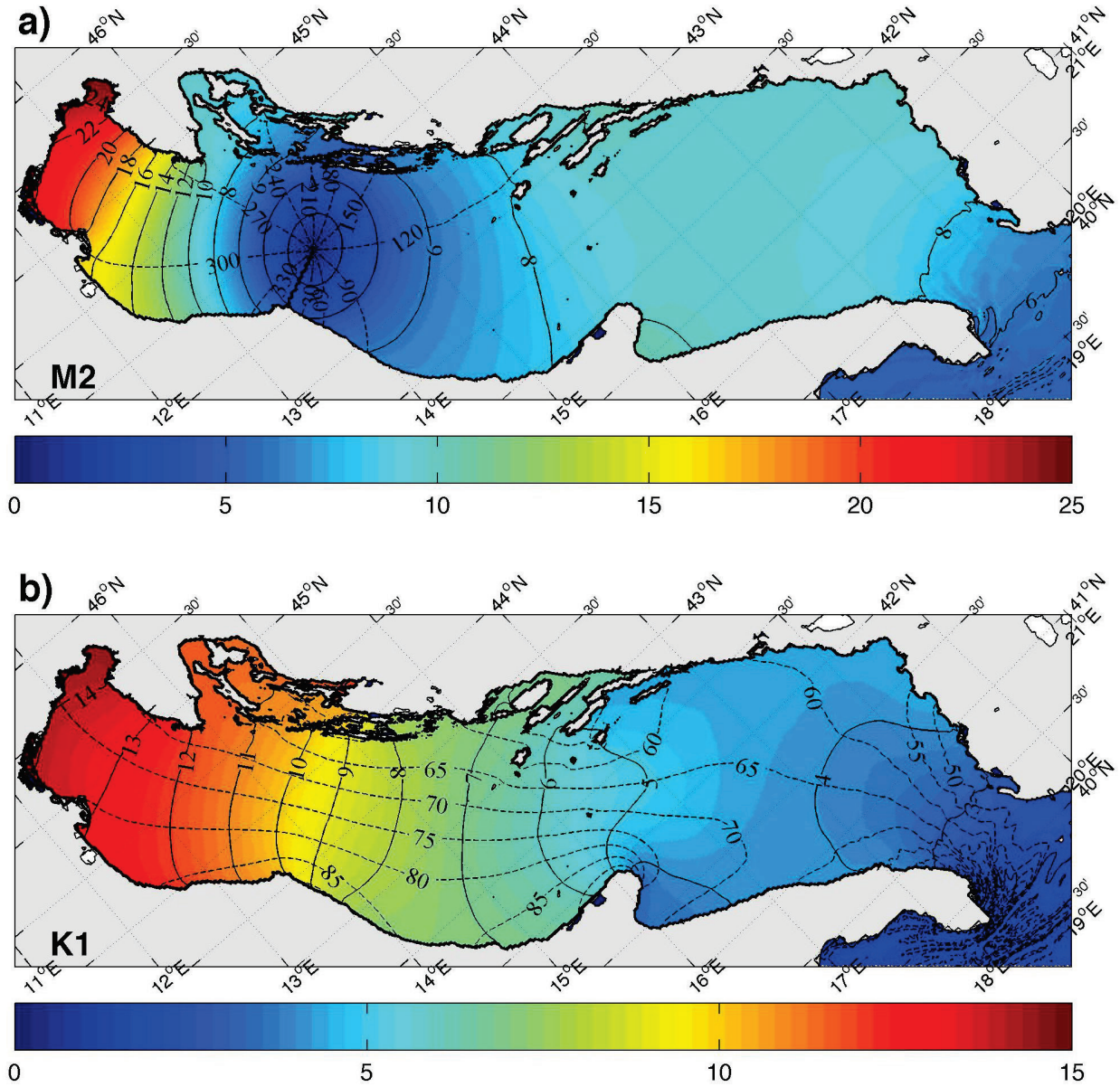

Figure 3. Panel a: temporal evolution of three depths for the model grid point nearest to Cape Struga (location shown by the blue diamond in Fig. 1 inlet). Panel b: same as panel a but reproduced from Fig. 2 of Mihanovic et al. [2006] at the location shown by the red dot in Fig. 1 inlet. Panel c: power spectral density of thermal variations at 30 m depth at diurnal frequency for the Adriatic basin.

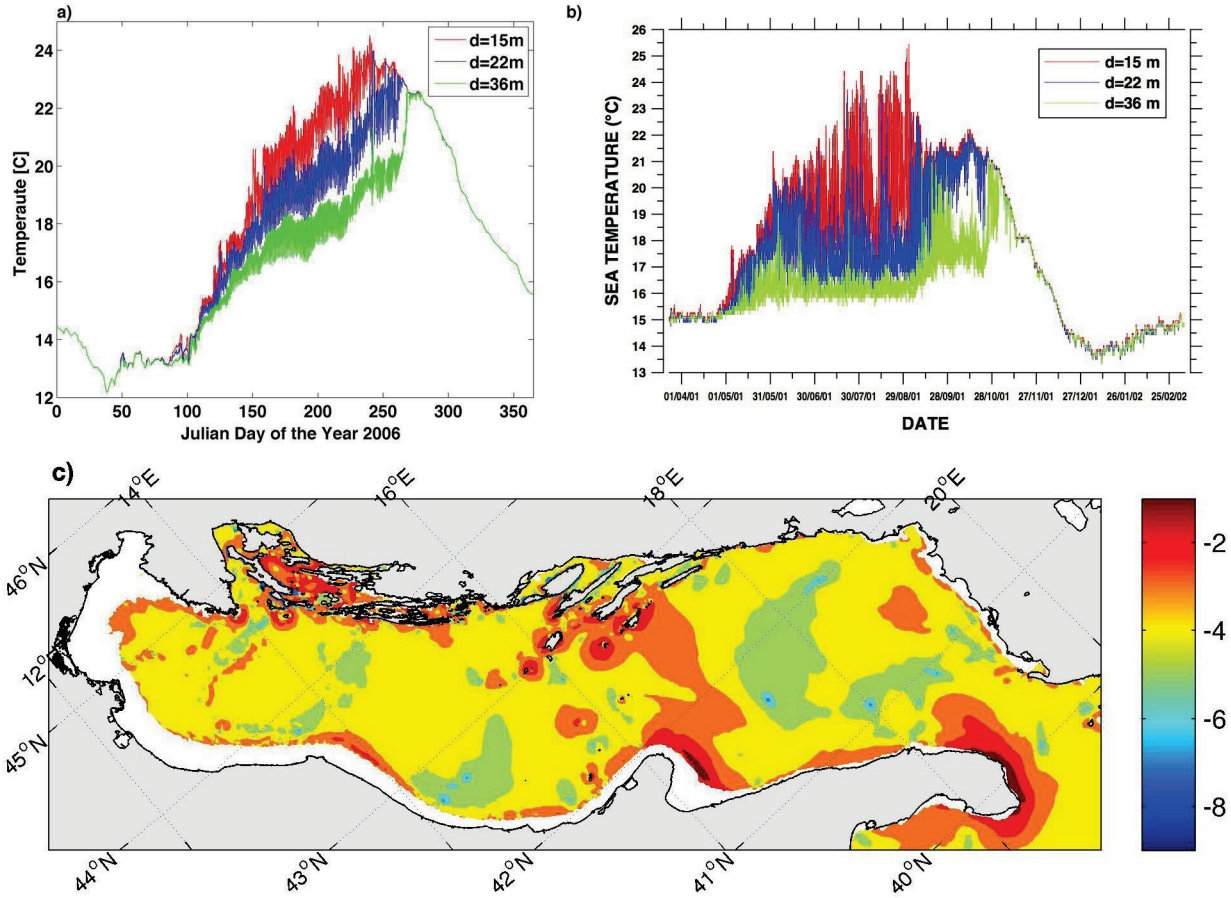

Figure 4. Panel a: temporal evolution in July of column temperature profile at the model grid point (location shown by green diamond in Fig 1) with tidal forcing at the boundary. Panel b: same as panel a except that it is a simulation without tidal forcing. Panel c: topographic slopes vs. critical slopes calculated along section 1 (location shown in Fig. 1), with the green line indicating the location of the model grid point time series of panels a and b. Panels d and e are the same as panels a and b, respectively, except that they are for the model grid point at the location shown by magenta diamond in Fig 1. Panel f is the same as panel c except that it is for section 2, with the magenta line indicating the location of the model grid point of interest for panels d and e.